Supplementary Materials for

Adaptive insertion of the hydrophobic anchor into poly(ethylene glycol) host for programmable surface functionalization

Shaohua Zhang[1], Wei Li[1], Jiabin Luan[1], Jiawei Sun[1], Danni Wang[1], Serena P. Teora[1], Daniela A. Wilson[1]*

[1]Radboud University Nijmegen, Institute for Molecules and Materials; Heyendaalseweg 135, 6525 AJ, Nijmegen, The Netherlands.

* Correspondence to: d.wilson@science.ru.nl

This PDF file includes:

Materials and Methods

Materials

Potassium hexachloroosmate(IV) (min 39% Os, K_2OsCl_6) and sodium dithionite ($Na_2S_2O_4$) were purchased from Acros Organics. 2,2′-Bipyridine (bpy), tetraethylene glycol (PEG_4), *p*-Toluenesulfonyl chloride (TsCl), imidazole, 1-bromo-2-methylpropane, benzyl bromide, 2-(bromomethyl)naphthalene, 1-(bromomethyl)pyrene, 1-pyrenecarboxylic acid (Py-COOH), 1-pyrenemethanol (Py-OH), sodium hydride (NaH, 60% dispersion in mineral oil), dicyclohexylcarbodiimide (DCC), poly(sodium 4-styrenesulfonate) (PSS, average M_w ~70000), poly(acrylic acid sodium salt) (PAA, average Mw ~5100), PEG (average M 380-420, BioUltra 1000, average M_n 2050 Da), indium tin oxide (nanopowder, 30 nm), fluorine-doped tin oxide (FTO) coated glass slide (surface resistivity ~7 Ω/sq), poly(ethylene glycol) diacrylate (PEGDA, M_n 575 Da), and 2-hydroxy-4′-(2-hydroxyethoxy)-2-methylpropiophenone (Irgacure 2959) were purchased from Sigma-Aldrich. Imidazole (Im) and cesium carbonate ($CeCO_3$) were purchased from Fluorochem Ltd. Water used in all experiments was deionized water produced by Millipore instrument.

Instruments

NMR spectra were collected on a Bruker 400 MHz Bruker Avance III spectrometer. MALDI-TOF was measured with Bruker Microflex LRF Maldi-tof system using alpha-Cyano-4-hydroxycinnamic acid (CHCA) as the matrix. The absorbance of the molecular probes was measured with JASCO V-630 UV-vis spectrophotometer. Cryo-EM was performed by JEOL TEM 2100. Fluorescence was measured with JASCO FP-8300ST Spectrofluorometer. ITC was measured with Auto-iTC200. Cyclic voltammograms were measured with Multi Autolab Series instruments (M101). SEM was measured with JEOL 6330 Cryo Field Emission Scanning Electron Microscope. Size and zeta potential of polymersomes were measured with Malvern DLS-Zetasizer. The concentration of polymersomes was measured with NanoSight LM10. Fluorescent microscopy images were taken with Leica DMi8 widefield microscope (excitation: 395 nm). Confocal z-stack images were taken with Leica SP8 AOBS-beamsplitting white-light laser confocal laser scanning microscope (excitation: 405 nm diode laser).

Synthesis of poly(ethylene glycol)-*b*-polystyrene (PEG_{44}-*b*-PS)

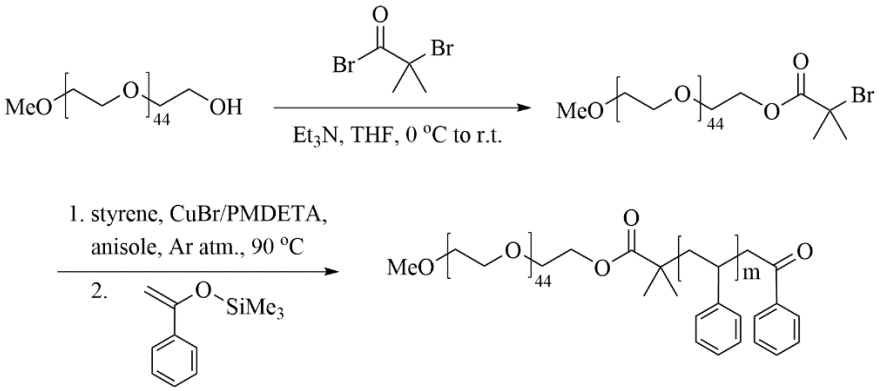

PEG_{44}-*b*-PS was synthesized by atom-transfer radical-polymerization (ATRP), as described in our previous publication[1]. The block copolymer was dissolved in $CDCl_3$ for ^{1}H-NMR. The length of PS was determined to be 178 by ^{1}H NMR spectrum. PDI of PEG_{44}-*b*-PS_{178} was 1.01 by GPC.

^{1}H-NMR (400 MHz, $CDCl_3$ with 0.05% v/v TMS): δ [ppm] = 7.24-6.28 (br. m, PS arom.), 3.64 (br. s, PEG backbone), 3.38 (s, 3H, CH_3-O-CH_2), 2.27-1.16 (br. m, PS backbone), 0.88 (br. m, 6H, C(O)-C(CH_3)$_2$-CH_2).

Synthesis of $[Os(bpy)_2Cl_2]$

K_2OsCl_6 (0.1 g, 0.21 mmol, 1 eq) and 2,2′-bipyridine (72 mg, 0.46 mmol, 2.2 eq) were dissolved in 5 mL dimethylformamide (DMF, 50 mL round bottom flask), which was heated under reflux for 6 h (140 °C, Ar). After cooling to room temperature, the mixture was centrifuged to remove the precipitate (KCl). The obtained supernatant was filled into a 500 mL flask and 50 mL diethyl ether was added dropwise under stirring. After 1 hour of stirring in an ice bath, the precipitate ($[Os(bpy)_2Cl_2]Cl$) was collected by centrifugation and dried.

$[Os(bpy)_2Cl_2]Cl$ was dissolved in a mixture of 1 mL DMF and 0.5 mL methanol. Solution of $Na_2S_2O_4$ (0.1 g, 0.57 mmol) in 10 mL water was added dropwise under stirring. The mixture was incubated in an ice bath to induce the crystallization of $[Os(bpy)_2Cl_2]$. $[Os(bpy)_2Cl_2]$ was collected by centrifugation, washed with H_2O, methanol, and ethanol, and dried (80 mg, 67%). $[Os(bpy)_2Cl_2]$ was dissolved in dichloromethane (DCM) for UV-vis measurement.

UV-vis (DCM): 240 nm (0.98, π → π* bpy), 298 nm (1.66, π → π* bpy), 383 nm (0.36, d → d Os^{2+}), 463 nm (0.33, d → d Os^{2+}), 558 nm (0.37, d → d Os^{2+})[2].

Synthesis of Hy-PEG_4-Os (3)

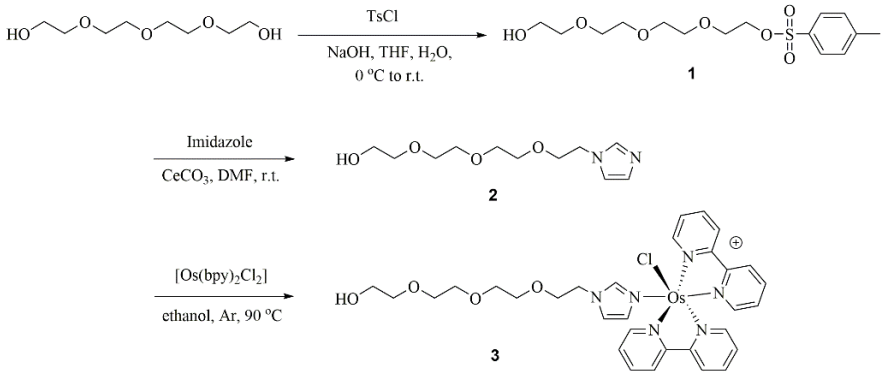

α-tosyl-ω-hydroxyl PEG (PEG_4-Ts, **1**). Tetraethylene glycol (PEG_4) (20 g, 103 mmol, 1.00 eq) was dissolved in 30 mL tetrahydrofuran (THF) and cooled to 0 °C. NaOH (1380 mg, 34 mmol, 0.33 eq) in 10 mL water was added, and the resulting mixture was stirred vigorously for 20 min. *p*-Toluenesulfonyl chloride (TsCl) (6.2 g, 32 mmol, 0.31 eq) in 35 mL THF was added dropwise over 2 h. The mixture was stirred under 0 °C for 2 h, and then under room temperature for 20 h. The mixture was then poured into 100 mL ice-cold water, which was extracted with DCM (4 ×25 mL). The combined organic layer was washed twice with water, and twice with saturated brine and dried with Na_2SO_4. The solid was filtered off, and the filtrate was concentrated under reduced pressure. The crude product was purified by column chromatography (ethyl acetate). PEG_4-Ts was obtained as viscous yellowish oil after dried in vacuo (6 g, 54%).

^{1}H-NMR (400 MHz, DMSO-d_6) δ [ppm] = 7.78 (d, 2H, Carom.H-C-SO_3), 7.48 (d, 2H, Carom.H-C-CH_3), 4.56 (t, 1H, -OH), 4.11 (t, 2H, CH_2-SO_3), 3.57 (t, 2H, C$\underline{H}_2$-CH_2-SO_3), 3.38-3.50 (m, 12H, (CH_2-CH_2-O)$_3$), 2.42 (s, 3H, -CH_3).

PEG_4-Imidazole (PEG_4-Im, **2**). PEG_4-Ts (2000 mg, 5.74 mmol, 1.0 eq), imidazole (312 mg, 4.58 mmol, 0.8 eq.), and $CeCO_3$ (392 mg, 17.22 mmol, 3 eq.) were added in 10 mL DMF. The mixture was stirred at room temperature for 2 days. The mixture was diluted with 30 mL DCM and filtrated to remove the solid. The mixture was washed with saturated $NaHCO_3$ (2×100 mL) and saturated brine (2×100 mL). The organic layer was dried over Na_2SO_4, and concentrated under reduced pressure. The crude product was purified by column chromatography (ethyl acetate → acetone), yielding a viscous colorless oil (890 mg, 80%).

^{1}H-NMR (400 MHz, DMSO-d_6) δ [ppm] = 7.62 (s, 1H, N-CH=N), 7.16 (s, 1H, N-CH=C$\underline{H}$-N), 6.86 (s, 1H, N-C$\underline{H}$=CH-N), 4.11 (t, 2H, CH_2-N), 3.67 (t, 2H, C$\underline{H}_2$-CH_2-N), 3.39-3.56 (m, 12H, (CH_2-CH_2-O)$_3$).

Hy-PEG$_4$-[Os(bpy)$_2$(Im)Cl] (Hy-PEG$_4$-Os, **3**). [Os(bpy)$_2$Cl$_2$] (33 mg, 0.058 mmol, 1 eq) and PEG$_4$-Im (12.8 mg, 0.052 mmol, 0.93 eq) was added in 8 mL ethanol, which was heated under reflux for 6 days (90 °C, Ar). After cooling to room temperature, the solvent was removed under reduced pressure, and the solid was dissolved in methanol. The obtained solution was centrifuged (14000 rpm, 2 min), and the supernatant was concentrated. Diethyl ether was added and the obtained solution was incubated in -20 °C, which was centrifuged to get the precipitates. The recrystallization was repeated for another time. After washing with diethyl ether and dried, PEG$_4$-Os was obtained as dark-red solid (36 mg, 88 %). Hy-PEG$_4$-Os was dissolved in DMSO-d_6 for ^{1}H-NMR (Fig. S3).

^{1}H-NMR (400 MHz, DMSO-d_6) δ [ppm] = for bpy 9.67 (d, 1H), 8.71 (d, 1H), 8.61 (d, 1H), 8.55 (d, 1H), 8.48 (d, 1H), 8.25 (d, 1H), 7.45-7.77 (m, 7H), 7.36 (d, H), 6.98-7.13 (m, 2H); for Im 7.83 (s, 1H), 7.21 (s, 1H), 6.44 (s, 1H); for PEG 4.56 (t, 1H, -OH), 4.12 (t, 2H, CH_2-N), 3.57 (t, 2H, $C\underline{H}_2$-CH_2-N), 3.36-3.52 (m, 12H, (CH_2-CH_2-O)$_3$).

MALDI-TOF MS: m/z=784.1 Da.

Synthesis of Pyrenyl-PEG$_4$-Os (Py-PEG$_4$-Os, 4)

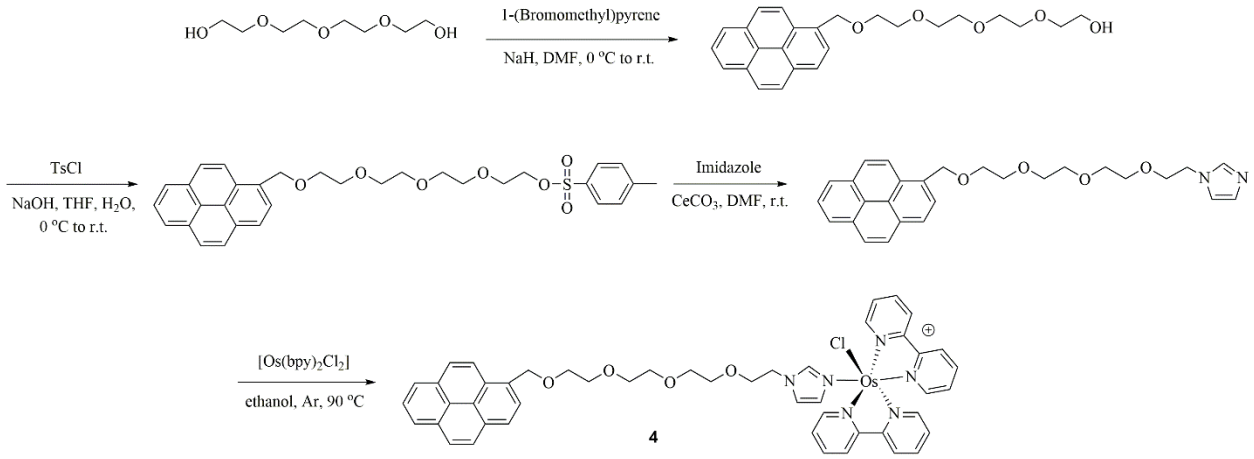

Py-PEG$_4$-Os was synthesized through a similar route as PEG$_4$-Os, where an additional step for the synthesis of Py-PEG$_4$ was added. Briefly, PEG$_4$ (970 mg, 5 mmol, 1 eq) was dissolved in 10 mL DMF, which was cooled to 0 °C with an ice bath. NaH (100 mg, 2.5 mmol, 0.5 eq), washed by heptane, was added to the reaction solution. After stirred for 30 min at 0 °C, 1-(bromomethyl)pyrene (502 mg, 2 mmol, 0.4 eq) was added. The mixture was stirred at 0 °C for 1 h, and stirred at room temperature for 24 h. The reaction was stopped by adding methanol and

water. The mixture was extracted with DCM (3 ×25 mL), and the combined organic layer was washed with saturated $NaHCO_3$ (2×50 mL) and saturated brine (2×50 mL). The organic layer was dried with Na_2SO_4, and concentrated under reduced pressure. The crude product was purified by column chromatography (DCM → ethyl acetate), yielding a viscous brown oil (613 mg, 75%). This product was used for the subsequent reaction without further purification according to similar conditions used for the synthesis of PEG_4-Os. Py-PEG_4-Os was dissolved in $CDCl_3$ for ^{1}H-NMR (Fig. S4).

^{1}H-NMR of Py-PEG_4-Os (400 MHz, $CDCl_3$) δ [ppm] = for bpy 9.77 (d, 1H), 8.60 (d, 1H), 8.53 (d, 1H), 8.38 (d, 1H), 8.33 (d, 1H), 7.98-8.23 (m, 1H), 7.29-7.63 (m, 8H), 6.91-7.02 (m, 1H), 6.86 (t, 1H); for Im 7.92 (s, 1H), 6.91-7.02 (m, 1H), 6.48 (s, 1H); for PEG 5.26 (s, 2H, Py-CH_2-O), 4.00 (t, 2H, CH_2-N), 3.40-3.80 (m, 14H, PEG backbone).

MALDI-TOF MS: m/z=998.9 Da

Synthesis of Isopropyl/Phenyl/Naphthyl-PEG_4-Os (Ip/Ph/Na-PEG_4-Os)

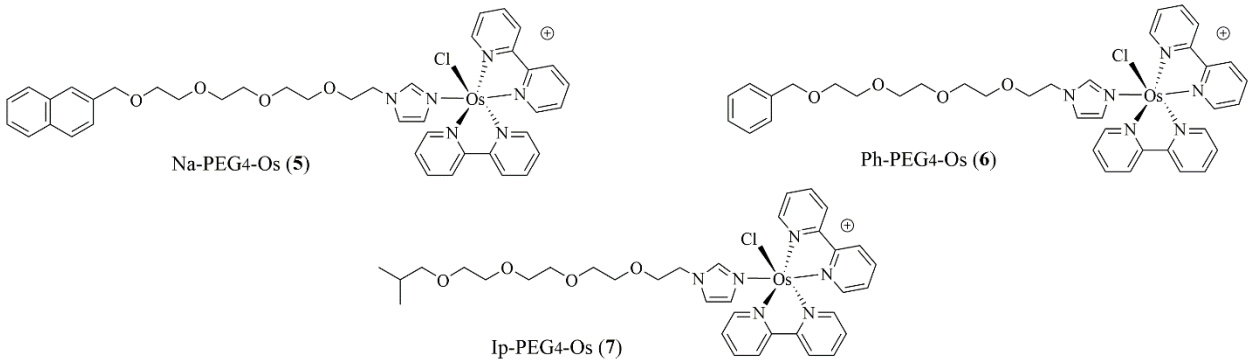

Ip/Ph/Na-PEG_4-Os were synthesized through a similar route as Py-PEG_4-Os.

Na-PEG_4-Os (**5**). ^{1}H-NMR (400 MHz, $CDCl_3$) δ [ppm] = for bpy 9.79 (d, 1H), 8.68 (d, 1H), 8.59 (d, 1H), 8.36 (d, 1H), 8.27 (d, 1H), 8.12 (d, 1H), 7.35-7.66 (m, 8H), 6.97 (t, 1H), 6.87 (t, 1H); for Im 7.95 (s, 1H), 7.03 (s, 1H), 6.50 (s, 1H); for Na 7.76-7.85 (m, 4H); 7.44-7.48 (m, 3H); for PEG 4.70 (s, 2H, N-CH_2-O), 4.09 (t, 2H, CH_2-N), 3.43-3.73 (m, 14H, PEG backbone) (Fig. S5).

MALDI-ToF MS: m/z=924.8 Da.

Ph-PEG_4-Os (**6**). ^{1}H-NMR (400 MHz, $CDCl_3$) δ [ppm] = for bpy 9.82 (d, 1H), 8.71 (d, 1H), 8.62 (d, 1H), 8.39 (d, 1H), 8.33 (d, 1H), 8.17 (d, 1H), 7.38-7.70 (m, 8H), 7.00 (t, 1H), 6.90 (t, 1H);

for Im 7.97 (s, 1H), 7.07 (s, 1H), 6.52 (s, 1H); for Ph 7.36-7.29 (m, 5H); for PEG 4.55 (s, 2H, Ph-CH_2-O), 4.13 (t, 2H, CH_2-N), 3.45-3.74 (m, 14H, PEG backbone) (Fig. S6).

MALDI-ToF MS: m/z=874.4 Da.

Ip-PEG$_4$-Os (**7**). ^{1}H-NMR (400 MHz, $CDCl_3$) δ [ppm] = for bpy 9.81 (d, 1H), 8.72 (d, 1H), 8.64 (d, 1H), 8.39 (d, 1H), 8.29 (d, 1H), 8.13 (d, 1H), 7.37-7.70 (m, 8H), 7.00 (t, 1H), 6.89 (t, 1H); for Im 7.96 (s, 1H), 7.07 (s, 1H), 6.56 (s, 1H); for Ip 1.85 (m, 1H), 0.88 (d, 6H); for PEG 4.16 (t, 2H, CH_2-N), 3.48-3.76 (m, 14H, PEG backbone), 3.20 (d, 2H, Ip-CH_2-O) (Fig. S7).

MALDI-ToF MS: m/z=840.3 Da.

Synthesis of Pyrenyl-Os (Py-Os, 8)

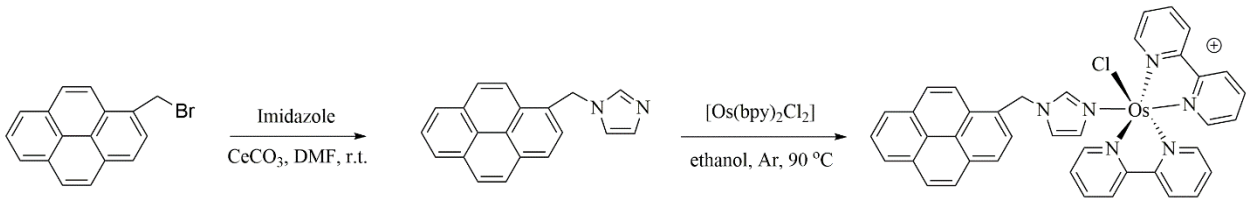

8

1-(bromomethyl)pyrene (59 mg, 0.2 mmol, 1.0 eq) was dissolved in 2 mL DMF. Imidazole (11 mg, 0.16 mmol, 0.8 eq.) and $CeCO_3$ (196 mg, 0.6 mmol, 3 eq.) was added. After stirring for 24 h, DCM was added and the resulting dispersion was filtrated to remove the salt. Py-Im was purified by column chromatography (DCM→DCM/methanol, 9:1 v/v). Py-Os was prepared by refluxing Py-Im and $[Os(bpy)_2Cl_2]$ in ethanol.

^{1}H-NMR (400 MHz, $CDCl_3$) δ [ppm] = for bpy 9.61 (d, 1H), 8.40 (d, 1H), 8.36 (d, 1H), 8.26 (d, 1H), 7.90 (d, 1H), 7.82 (d, 1H), 7.48-7.58 (m, 2H), 7.27-7.42 (m, 5H), 7.12 (t, 1H), 6.84 (t, 2H); for Im 7.70 (s, 1H), 6.96 (s, 1H), 6.65 (s, 1H); for Py 8.27-8.33 (m, 3H), 8.04-8.18 (m, 6H), 5.87 (q, 2H, Py-CH_2-N).

Synthesis of Py-PEG$_4$-Os (ester) (9)

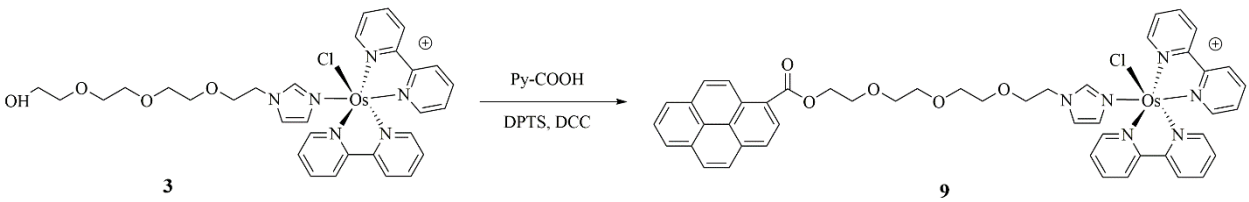

3 **9**

Hy-PEG$_4$-Os (3.9 mg, 0.005 mmol, 1 eq.), Py-COOH (3.7 mg, 0.015 mmol, 3 eq.), DPTS (0.75 mg, 0.0025 mmol, 0.5 eq.), and DCC (2 mg, 0.01 mmol, 2 eq.) was added to 0.5 mL anhydrous DCM. After stirring for 40 h, the reaction solution was filtrated. Py-PEG$_4$-Os (ester) was purified by column chromatography and recrystallization in cold diethyl ether. After washing with diethyl ether and dried, Py-PEG$_4$-Os (ester) was obtained as a dark-red solid (4.6 mg, 91%).

^{1}H-NMR (400 MHz, $CDCl_3$) δ [ppm] = for bpy 9.27 (d, 1H), 8.64 (d, 1H), 8.57 (d, 2H), 8.05-8.32 (m, 1H), 7.84 (s, 1H), 7.30-7.81 (m, 8H), 6.85 (t, 1H), 6.72 (d, 1H); for Im 7.86 (s, 1H), 7.02 (s, 1H), 6.56 (s, 1H); for PEG 4.66 (t, 2H,), 4.05 (t, 2H), 3.96 (t, 2H), 3.43-3.79 (m, 10H).

Synthesis of Py-PEG$_{11}$-Os (ester) and Py-PEG$_{21}$-Os (ester)

Py-PEG$_{11}$-Os (ester) and Py-PEG$_{21}$-Os (ester) were prepared through the same route as Py-PEG$_4$-Os (ester). PEG with a molecular weight of 400 and 1000 Da was used for tosylation. Monotosylated PEG was purified by column chromatography (ethyl acetate → acetone), which was confirmed by MALDI-TOF. As-prepared monotosylated PEG was used for the synthesis of Py-PEG$_{11}$-Os and Py-PEG$_{21}$-Os (ester).

MALDI-TOF

1 uL of sample solution (water, 2 mg mL^{-1}), 15 ul of CHCA (ethanol, 10 mg mL^{-1}), and 4 uL of NaTFA (water, 10 mg mL^{-1}) were mixed. 1 μL of the mixed solution was spotted onto the MALDI plate, which was dried before being inserted into the instrument for analysis.

Preparation of PEG hydrogel microparticles

All of the solutions were flushed with nitrogen for 0.5 h to remove dissolved oxygen. The fluorocarbon oil (HFE 7500) and the PEGDA (40% w/w) were injected respectively in the first and second inlet of the PDMS microfluidic device. Irgacure 2959 (0.4 wt% final concentration) was added to the PEGDA solution before injection. The droplets were formed at the cross-junction by the introduction of an outer phase consisting of fluorocarbon oil (HFE 7500) and surfactant (SS01, 1% w/w). The resulting emulsion was collected in an Eppendorf and then UV cured by exposure to a focused UV beam (λ = 320-500 nm, 5 min, 60% intensity). The emulsion was broken by adding 1H,1H,2H,2H-Perfluoro-1-octanol (100μL, 20% w/w in hexane), after which the

microparticles were washed with Milli-Q. Flow rates were 600 μL h^{-1} for fluorocarbon oil, and 60 μL h^{-1} for PEGDA.

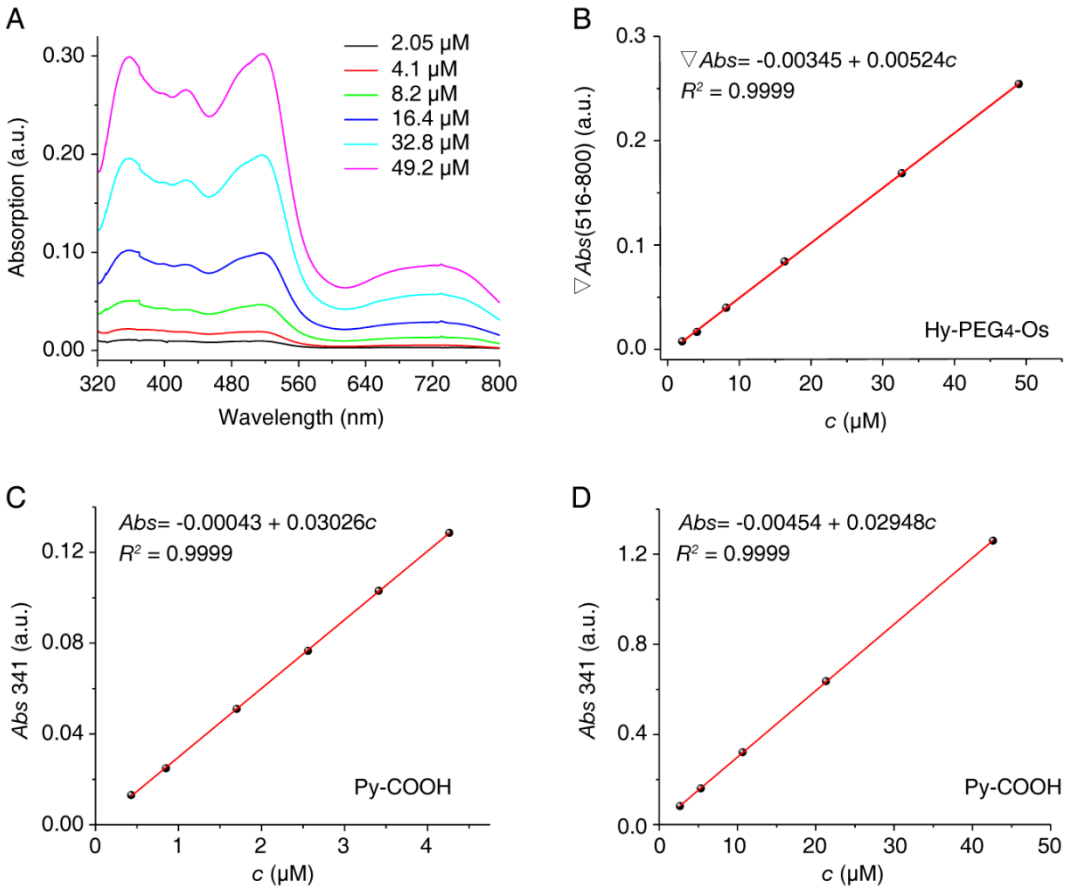

Figure S1. (**A**) UV-vis spectra of different concentrations of Hy-PEG$_4$-Os in water. (**B**) The plot of the absorption difference between 516 nm and 800 nm (▽*Abs*(516-800)) of Hy-PEG$_4$-Os in water as a function of concentration. (**C, D**) Representative plot of the absorption at 341 nm of Py-COOH in water (pH=7.0) as a function of concentration.

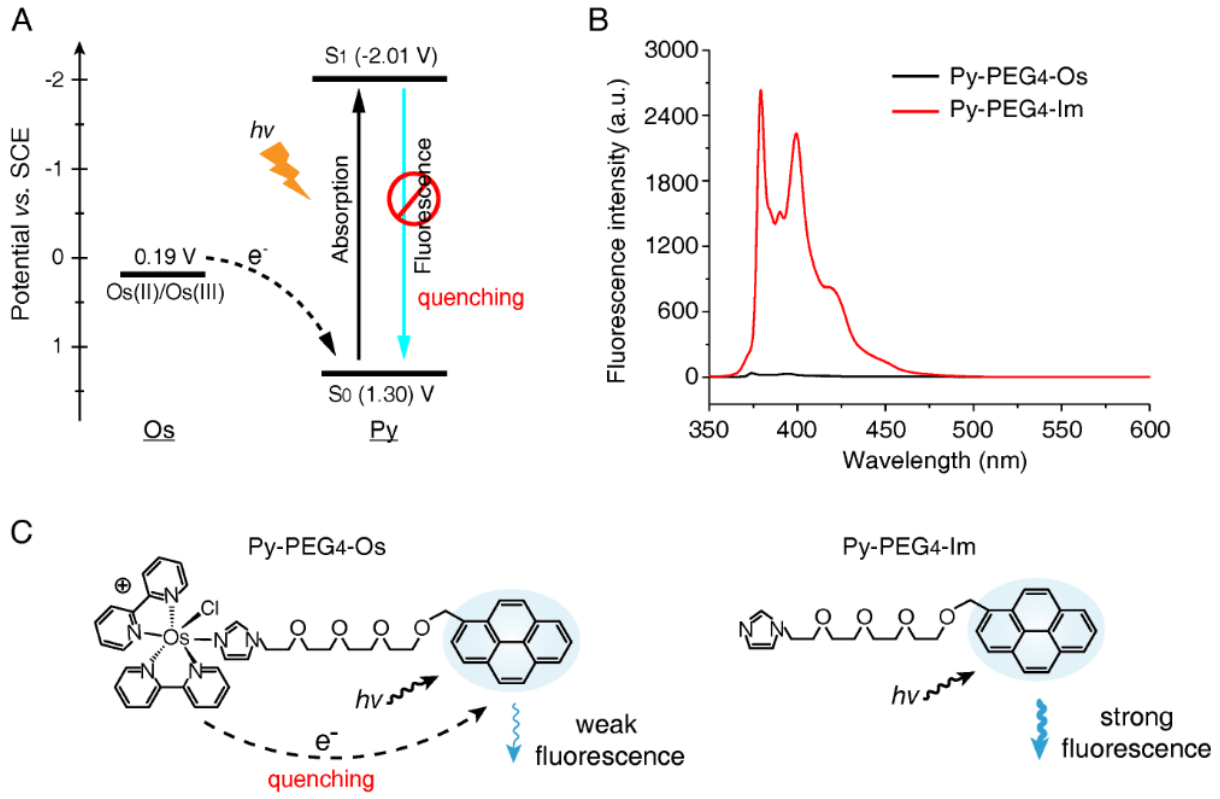

Figure S2. (**A**) Schematic fluorescence quenching of Py by photoinduced electron transfer from Os to Py[3,4]. (**B**) Fluorescence of 1.51 uM Py-PEG$_4$-Os and Py-PEG$_4$-Im. (**C**) Schematic fluorescence of Py-PEG$_4$-Os and Py-PEG$_4$-Im.

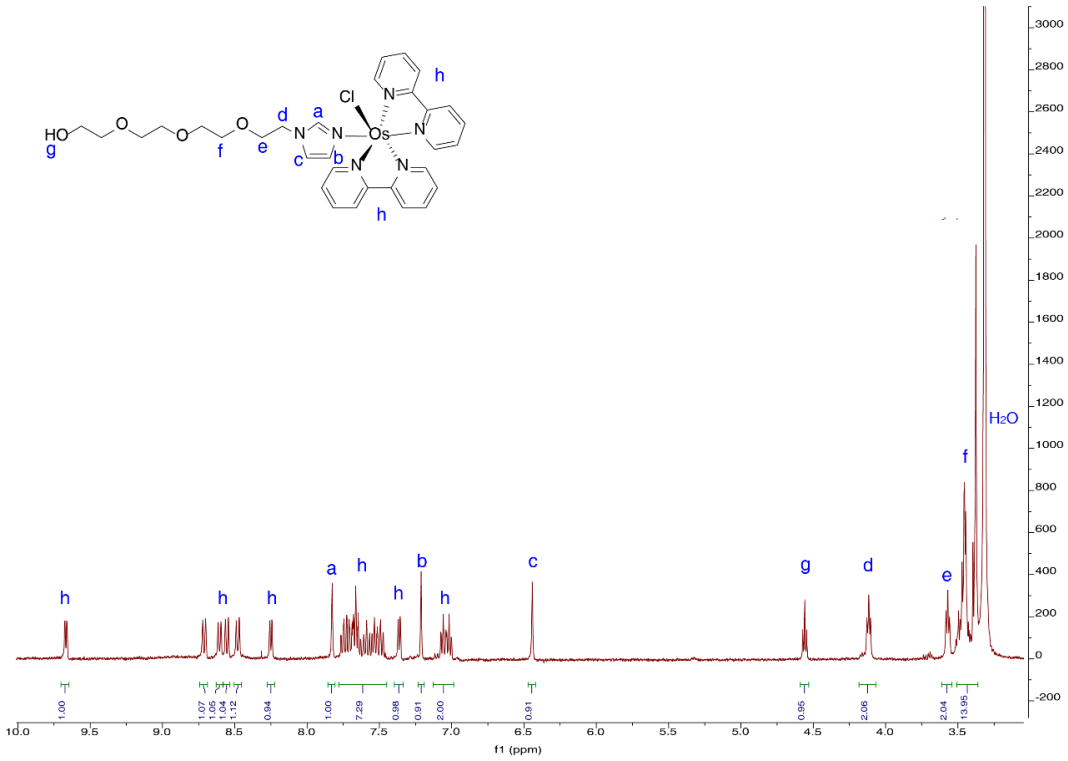

Figure S3. ^{1}H-NMR spectrum of Hy-PEG$_4$-Os in DMSO-d_6.

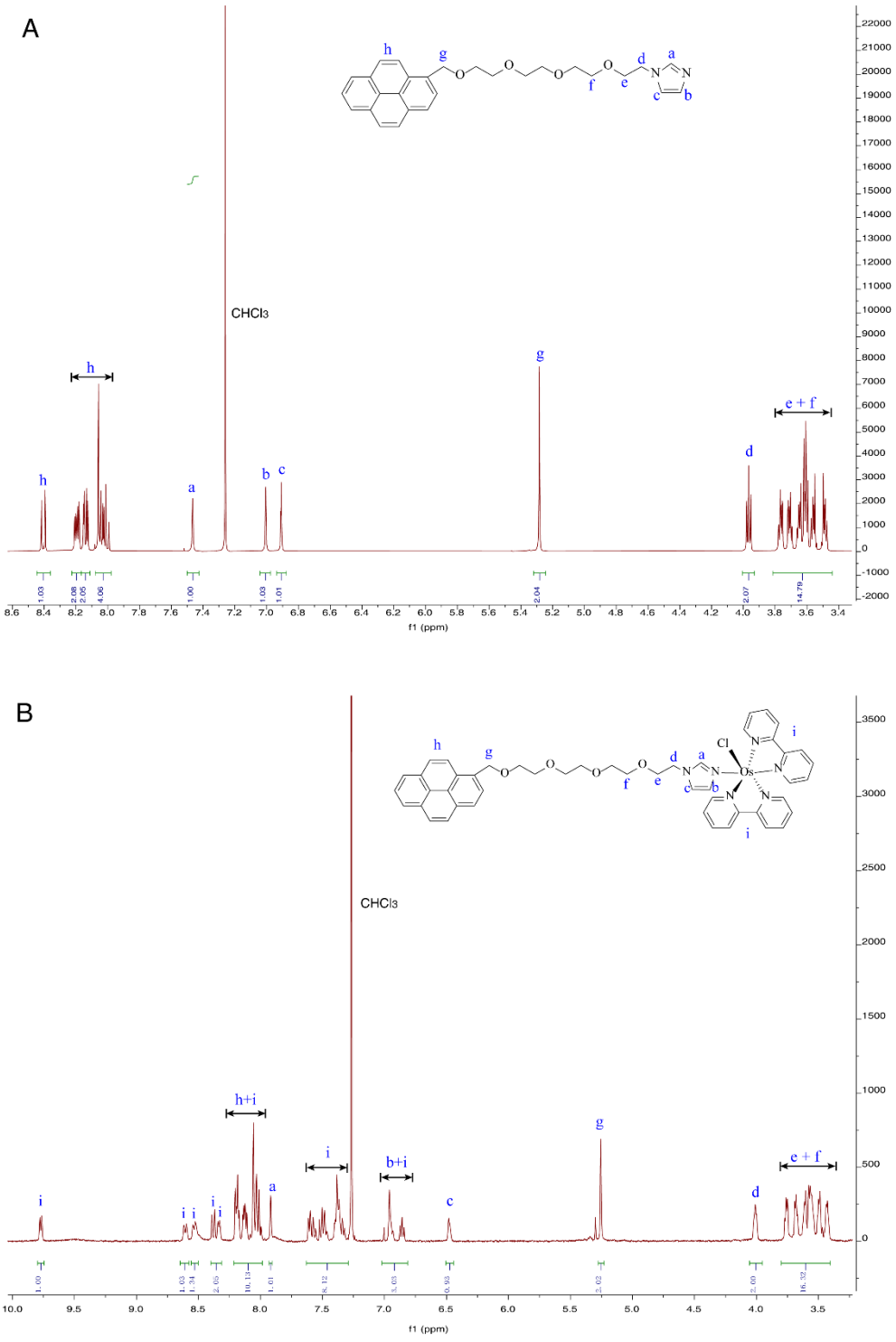

Figure S4. ^{1}H-NMR spectra of (**A**) Py-PEG$_4$-Im and (**B**) Py-PEG$_4$-Os in CDCl$_3$.

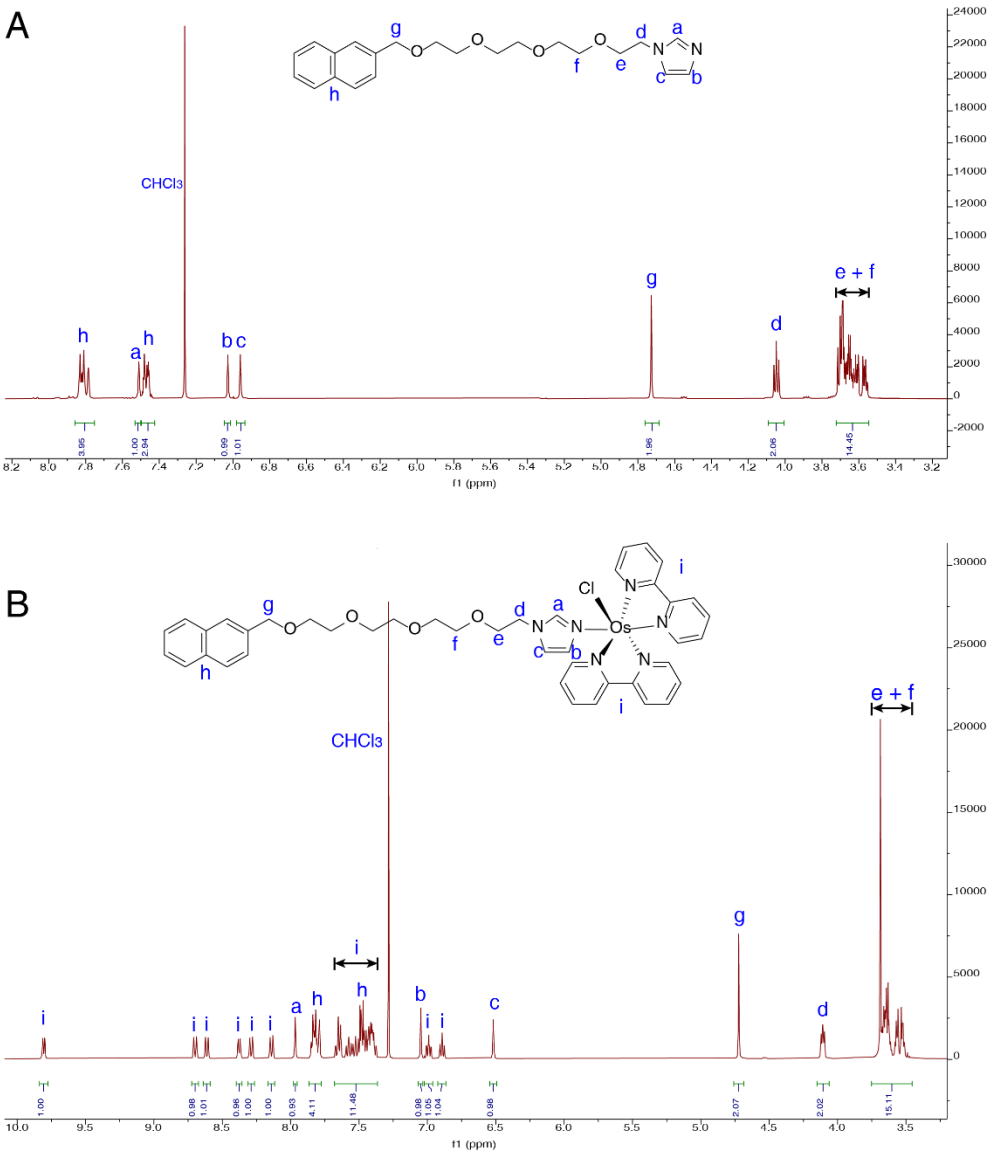

Figure S5. ^{1}H-NMR spectra of (**A**) Na-PEG$_4$-Im and (**B**) Na-PEG$_4$-Os in $CDCl_3$.

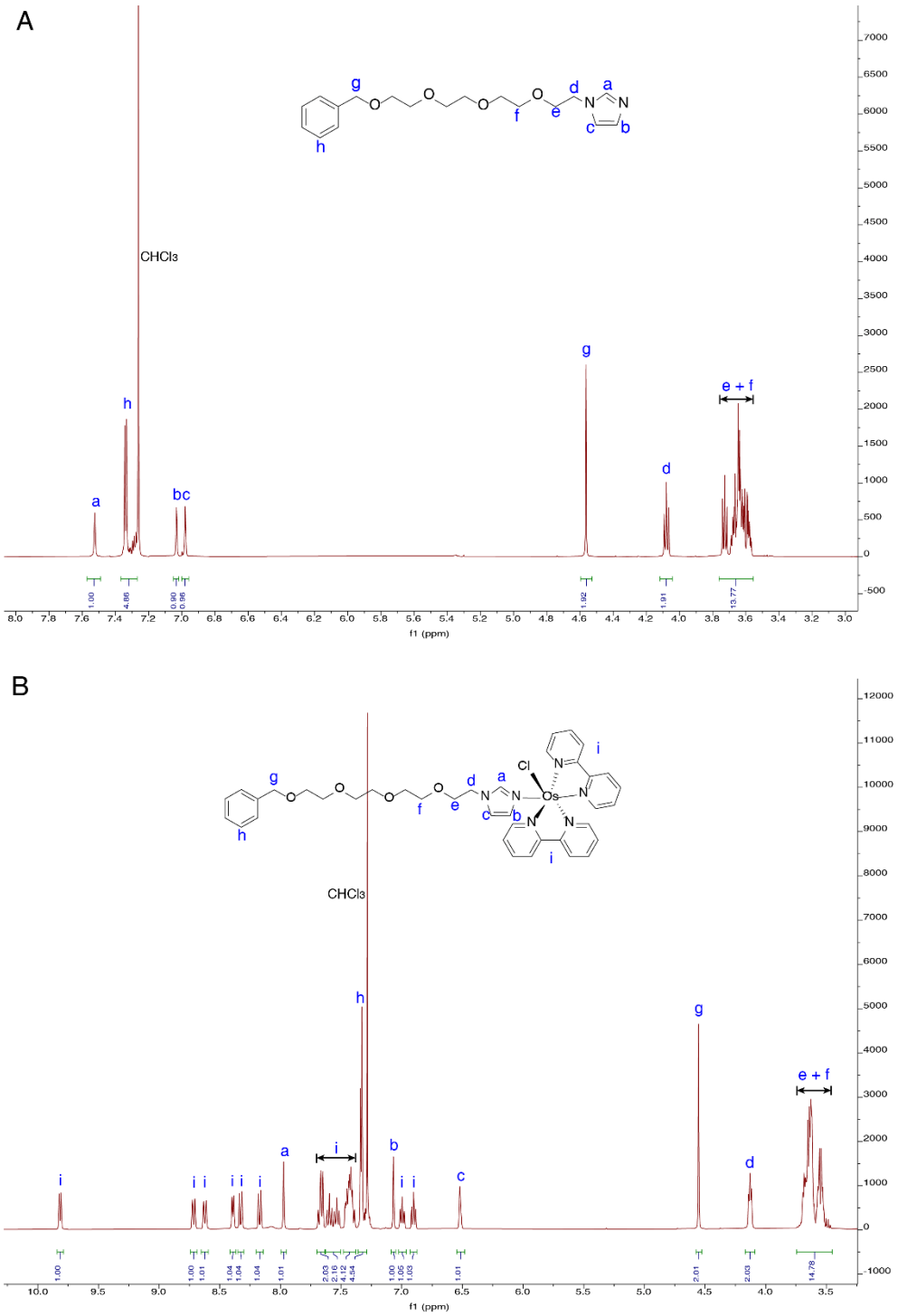

Figure S6. ^{1}H-NMR spectra of (**A**) Ph-PEG$_4$-Im and (**B**) Ph-PEG$_4$-Os in $CDCl_3$.

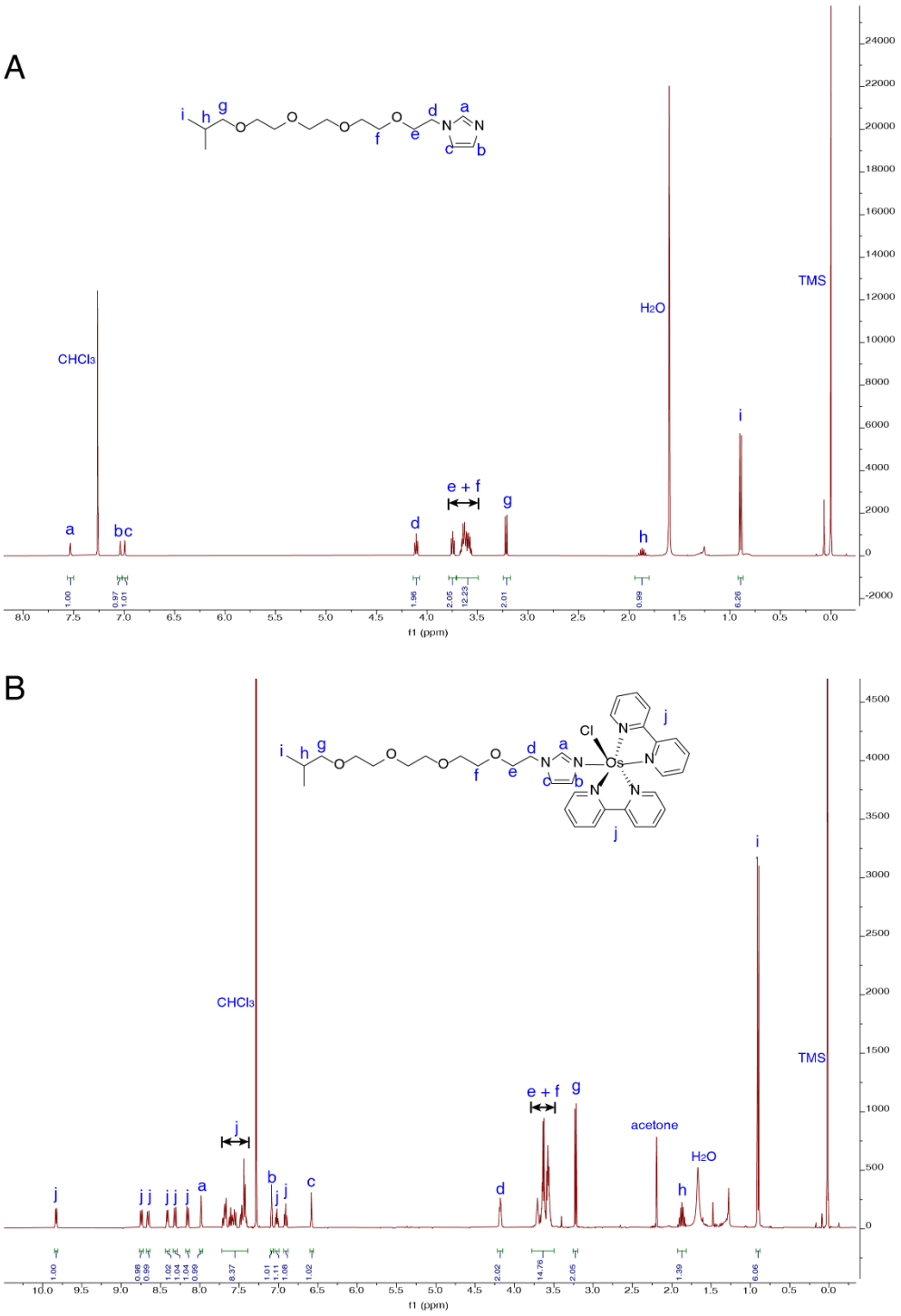

Figure S7. ^{1}H-NMR spectrum of (**A**) Ip-PEG$_4$-Im and (**B**) Ip-PEG$_4$-Os in $CDCl_3$.

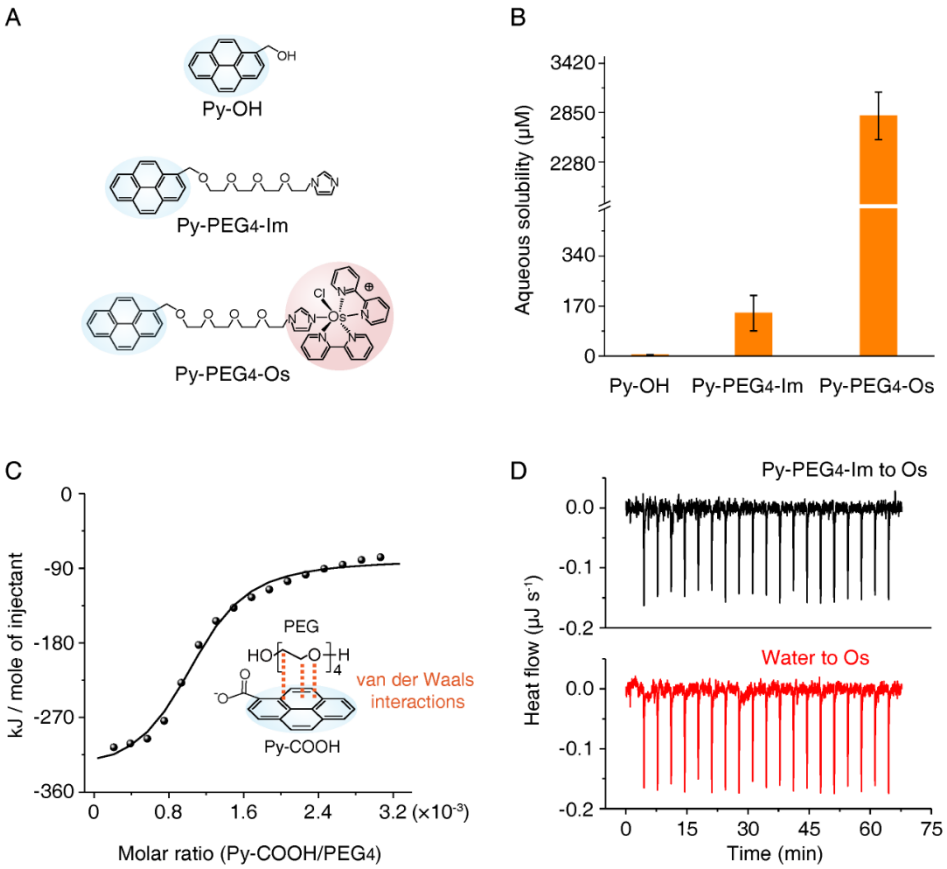

Figure S8. (**A**) Chemical structure and (**B**) aqueous solubility of Py-OH, Py-PEG$_4$-Im, and Py-PEG$_4$-Os. (**C**) ITC analysis of the interaction between Py-COOH and PEG$_4$. 133 uM Py-COOH solution (pH=7.0) was injected into 7.5 mM PEG$_4$ for ITC measurement. (**D**) ITC analysis of the interaction between Py-PEG$_4$-Im and Os in water. 146 uM Py-PEG$_4$-Im was injected into 397 uM Os for ITC measurement. No interaction between Os and Py-PEG$_4$-Im was detected.

Section 1. Aqueous solubility of molecular probes

Once linked to -PEG_4-Os with ether group, hydrophobic Py can be easily dissolved in water. Specifically, the solubility of Py-PEG_4-Os reached 2812±275 μM at room temperature, which was ~700 fold of Py-OH (4±1 μM) (Fig. S8). This should arise from the 1) intramolecular van der Waals interaction between PEG spacer and Py, which reduced the unfavorable interaction between Py and water, 2) intermolecular electrostatic repulsion between positive charged Os, which inhibited the aggregation of Py in water. When Py was linked to electrically neutral -PEG_4-Im, the solubility was increased from 4±1 μM to 146±60 μM, confirming the role of PEG spacer in increasing the solubility (Fig. S8). When Os was attached to Py-PEG_4-Im, the solubility of Py was further increased to 2812±275 μM. Since Os did not interact with Py or PEG (Fig. S8). Thus, intermolecular electrostatic repulsion between positively charged Os should contribute to the high solubility of Py-PEG_4-Os.

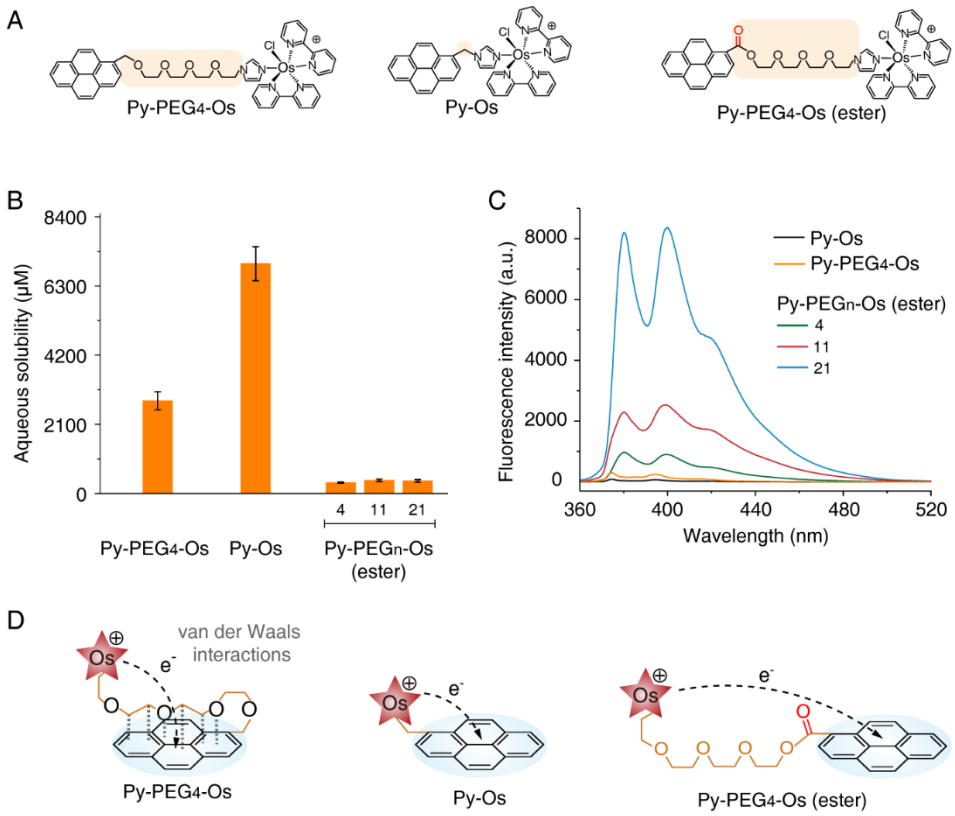

Figure S9. (**A**) Chemical structure and (**B**) aqueous solubility of Py-Os, Py-PEG$_4$-Os, and Py-PEG$_4$-Os (ester). (**C**) Fluorescence of 11 μM Py-Os, Py-PEG$_4$-Os, and Py-PEG$_n$-Os (ester). (**D**) Schematic molecular conformation of Py-Os, Py-PEG$_4$-Os, and Py-PEG$_4$-Os (ester) in water.

S2. Conformation of molecular probes dissolved in water

To investigate molecular conformation, we synthesized three different molecular probes, including Py-PEG$_4$-Os, Py-Os, and Py-PEG$_4$-Os (ester) (Fig. S9). Aqueous solubility and fluorescence of Py were measured to validate the molecular conformation. Since electrostatic repulsion between Os mainly contributed to the aqueous solubility, a larger distance between Py and Os should lead to the lower solubility of the molecular probe. The solubility decreased in the order of Py-Os＞Py-PEG$_4$-Os＞Py-PEG$_4$-Os (ester), suggesting that the distance between Py and Os increased in the order of Py-Os＜Py-PEG$_4$-Os＜Py-PEG$_4$-Os (ester) (Fig. S9).

The distance between Py and Os was further investigated by measuring the fluorescence of Py. Os can quench the fluorescence of Py by photoinduced electron transfer from Os to Py (Fig. S2). Since electron transfer efficiency was negatively correlated with distance, the combination of Py and Os should provide a unique method to investigate the molecular conformation[5]. This method was first tested with Py-PEG$_n$-Os (ester), where the distance between Py and Os was controlled by increasing the length of the PEG spacer (n=4, 11, 21). As shown in Figure S9, the fluorescence intensity of Py got increased with the length of the PEG spacer. This demonstrated that the fluorescence intensity of Py was sensitive enough to reflect the distance between Py and Os. The fluorescence intensity of Py decreased in the order of Py-Os＜Py-PEG$_4$-Os＜Py-PEG$_4$-Os (ester), suggesting that the distance between Py and Os increased in the order of Py-Os＜Py-PEG$_4$-Os＜ Py-PEG$_4$-Os (ester). This was consistent with solubility experiments.

Based on the above results, we proposed the molecular conformation of Py-PEG$_4$-Os, Py-Os, and Py-PEG$_4$-Os (ester) in water (Fig. S9). Py-Os exhibited the shortest distance between Py and Os. When the PEG$_4$ spacer was introduced, the distance between Py and Os was enlarged. For Py-PEG$_4$-Os, Py-C(H2) bond could be rotated to enable the PEG spacer to partially cover Py by forming van der Waals interaction. This contributed to the folded conformation of Py-PEG$_4$-Os in water, which can reduce the unfavorable interaction between Py and water. For Py-PEG$_4$-Os (ester), the resonance interaction between carbonyl group (-C(=O)-) and Py would restrict the rotation of Py-C(=O) bond[6]. This should inhibit PEG spacer to interact with Py, and contribute to the extended conformation of Py-PEG$_4$-Os (ester). These molecular conformations should result in the different distances between Py and Os.

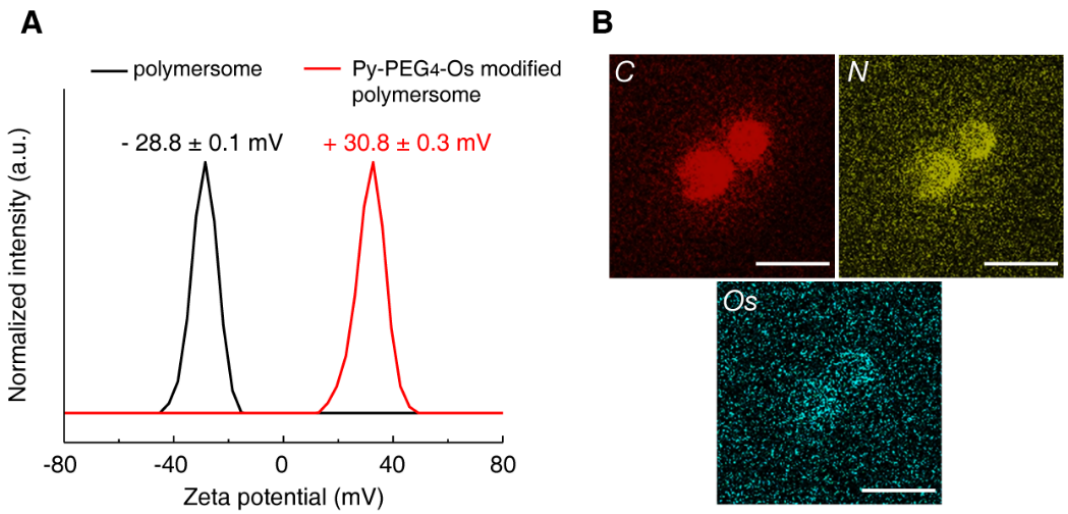

Figure S10. (**A**) Zeta potential of polymersomes before and after the modification by Py-PEG$_4$-Os. (**B**) Elemental mapping of polymersomes modified by Py-PEG$_4$-Os.

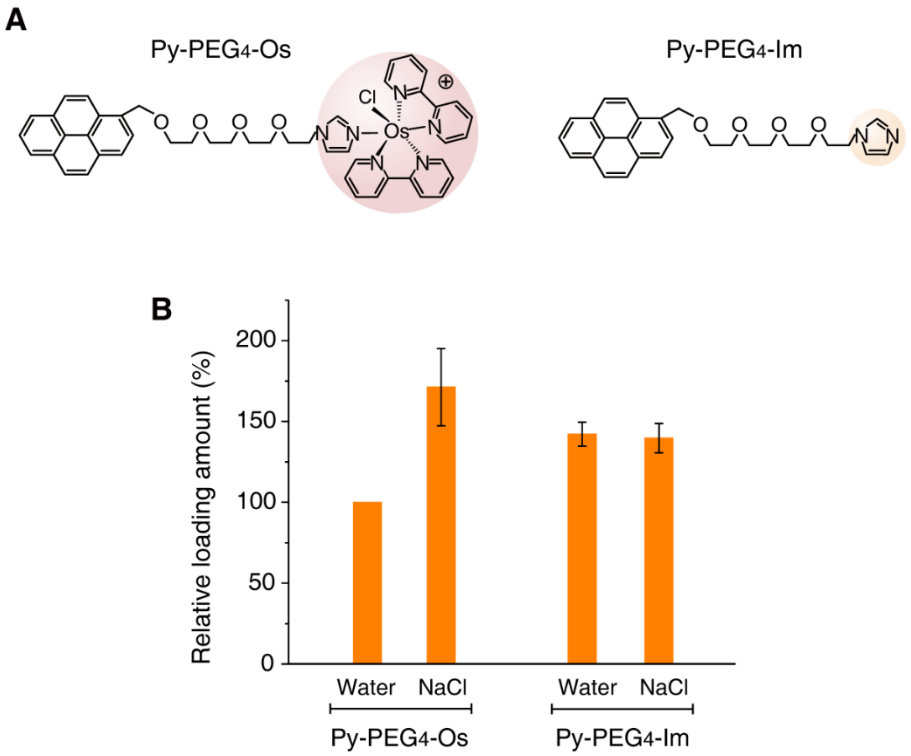

Figure S11. (**A**) Chemical structure of Py-PEG$_4$-Os and Py-PEG$_4$-Im. (**B**) The relative loading amount of Py-PEG$_4$-Os and Py-PEG$_4$-Im on polymersomes in water or 20 mM NaCl solution. In the presence of NaCl, the relative loading amount of Py-PEG$_4$-Os was increased from 100% to 171±24%. For electrically neutral Py-PEG$_4$-Im, the relative loading number was not influenced by NaCl. This suggested that electrostatic repulsion between Os was restricting the loading amount of Py-PEG$_4$-Os.

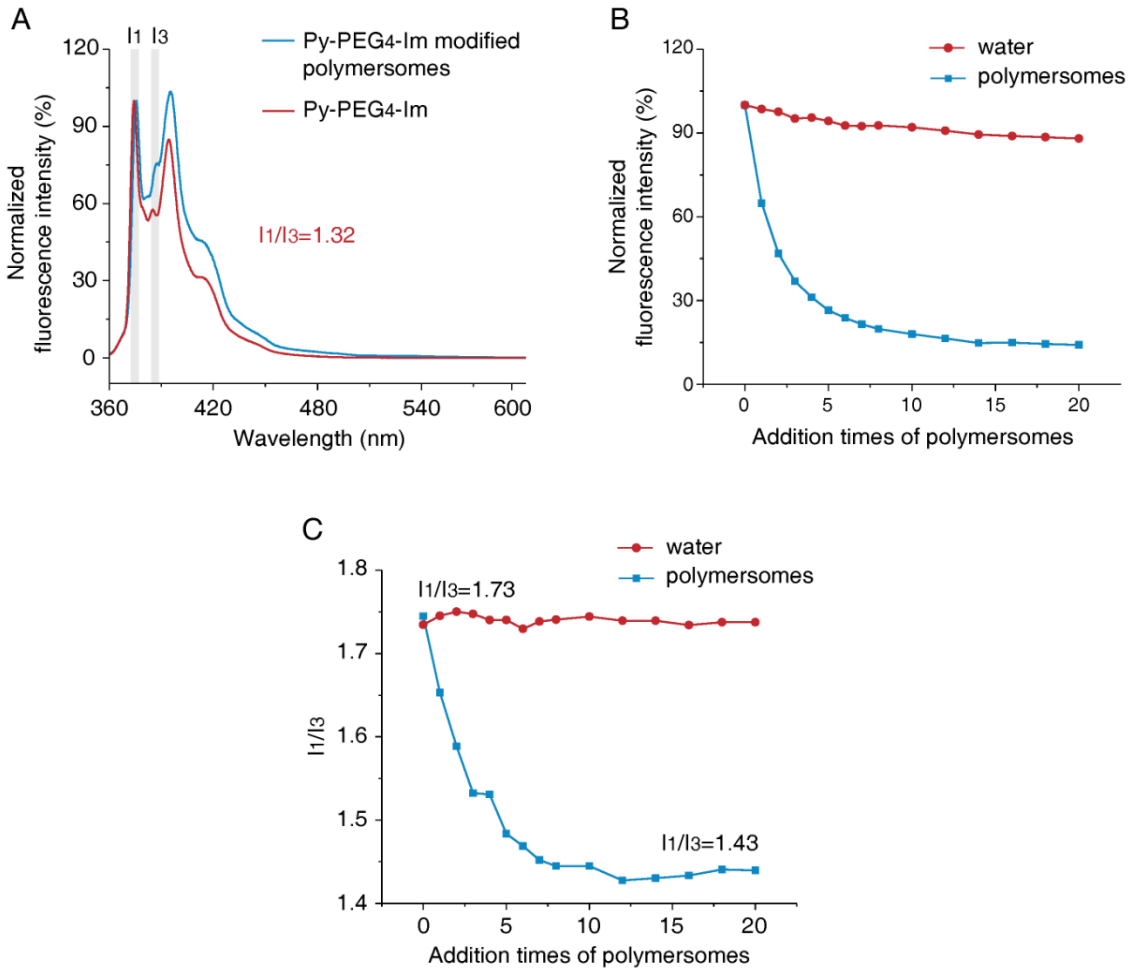

Figure S12. (**A**) Normalized fluorescence of Py-PEG$_4$-Im loaded onto polymersomes and dissolved in water, respectively. The fluorescence intensity was normalized at the first fluorescence peak (I_1). The ratio of the first and third fluorescence peaks (I_1/I_3) was calculated to reflect the medium polarity around Py. Change of (**B**) fluorescence intensity and (**C**) I_1/I_3 during the binding between Py-PEG$_4$-Im and polymersomes. 100 uL dispersion of polymersomes ($5.56\times10^{-9} \pm 2.2\times10^{-10}$ mol L^{-1}) or water was added to Py-PEG$_4$-Im (4.5 μM, 1.2 mL) in 20 times.

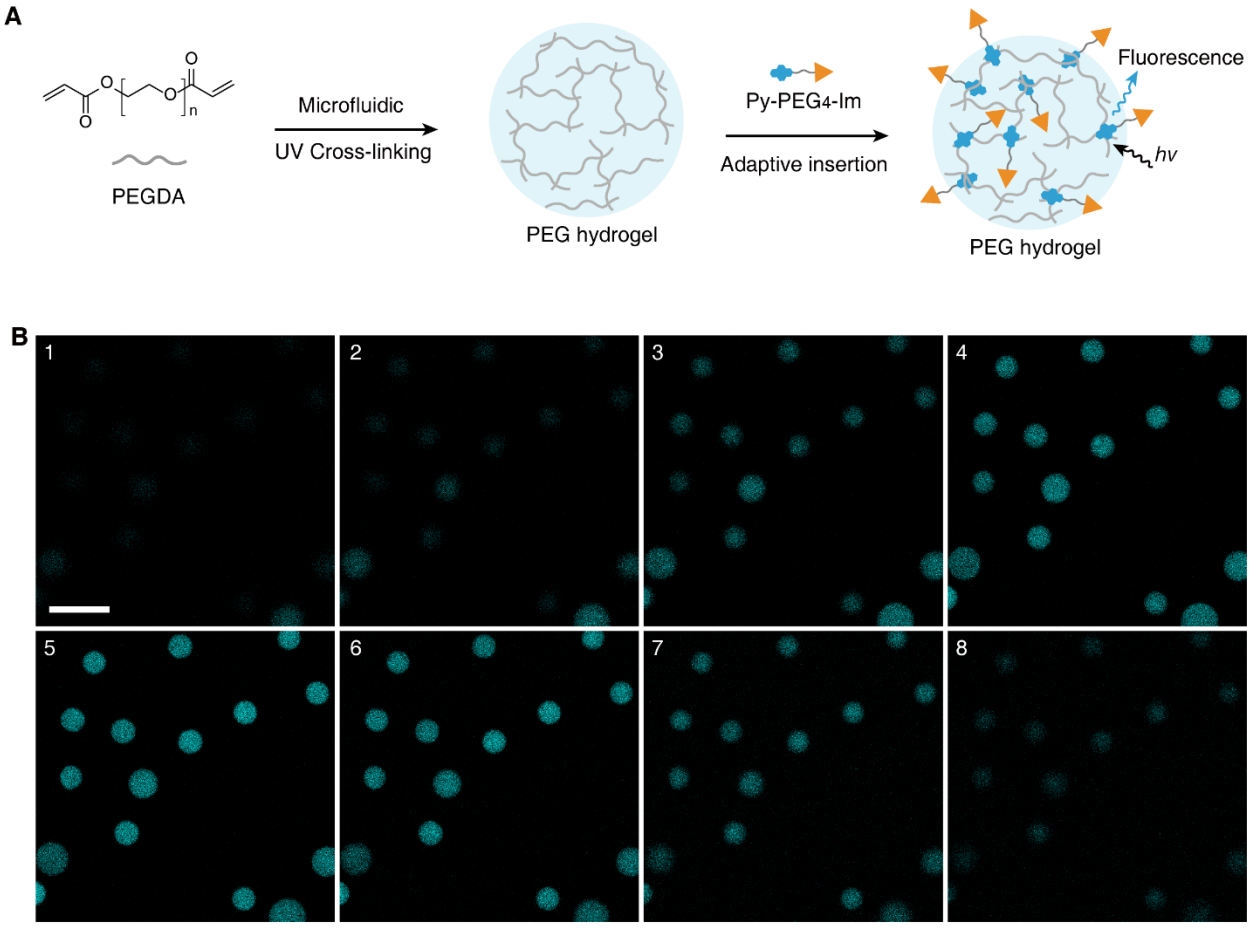

Figure S13. (**A**) Preparation and adaptive insertion of Py-PEG$_4$-Im into PEG hydrogel microparticles. (**B**) Confocal z-stack images of PEG hydrogel microparticles loaded with Py-PEG$_4$-Im. The image was taken every 4 μm along the z-axis. The PEG hydrogel microparticles were prepared by microfluidic setup as reported in our previous publication[7].

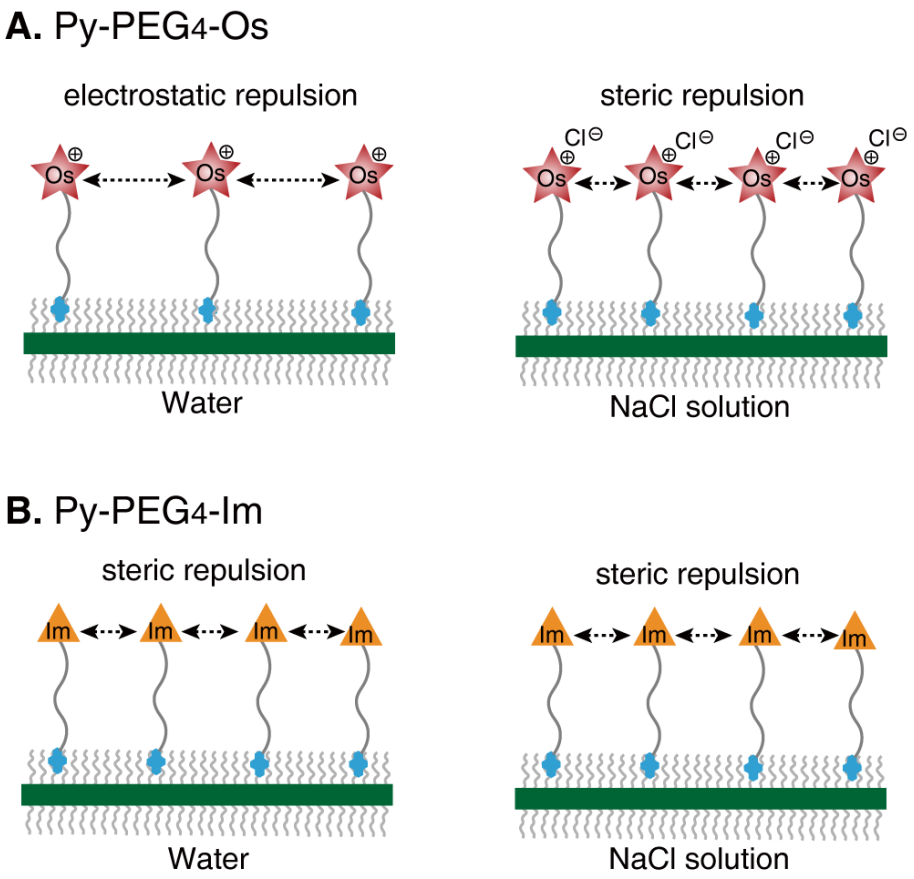

Figure S14. Schematic packing of (**A**) Py-PEG$_4$-Os and (**B**) Py-PEG$_4$-Im on PEG corona of polymersomes. Py-PEG$_4$-Os and Py-PEG$_4$-Im were loaded on polymersomes in water or 20 mM NaCl solution, respectively. Electrostatic repulsion between Os restricted the packing density of Py-PEG$_4$-Os on PEG corona. In the presence of 20 mM NaCl, the electrostatic repulsion was screened, resulting in a higher packing density of Py-PEG$_4$-Os on PEG corona. For Py-PEG$_4$-Im, steric repulsion between Py-PEG$_4$-Im should restrict the packing density on PEG corona, which was not influenced by NaCl.

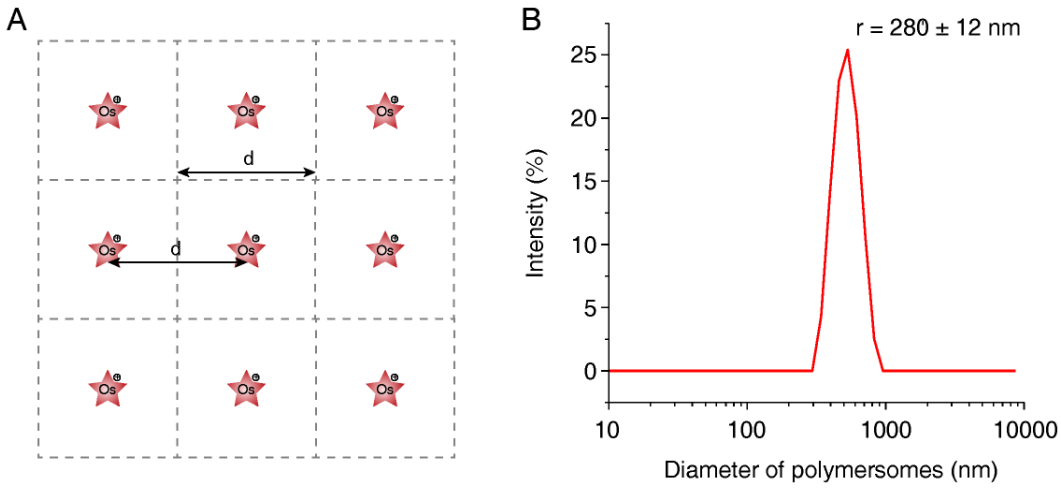

Figure S15. (**A**) Schematic distribution of Py-PEG$_4$-Os on PEG corona of polymersomes. Py-PEG$_4$-Os was loaded on polymersomes in water. (**B**) Dynamic light scattering (DLS) intensity size distribution of polymersomes dispersed in water.

Due to the electrostatic repulsion, Os should be homogenously distributed on the surface of the polymersomes. The separation distance between the adjacent Os was defined as d (Fig. S15A). The area occupied by each Os on the surface of the polymersomes was defined as a square (d × d). Based on the above assumption, d could be calculated by equation S1:

$$d = \sqrt{\frac{4\pi r^2}{n}} \qquad \text{(S1)}$$

where r is the radius of polymersomes, and n is the loading number of Os per polymersome. r was determined to be 280 ± 12 nm by DLS (Fig. S15B). n was determined by a UV-vis spectrometer. Thus, d was calculated to be 6.4±0.3 nm.

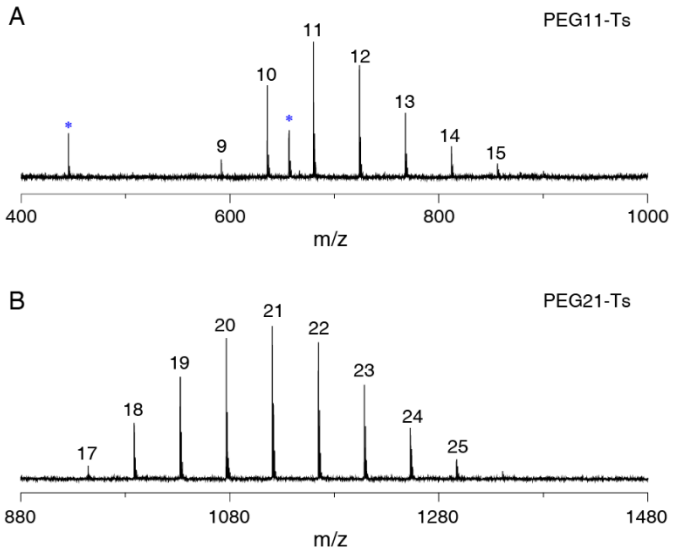

Figure S16. MALDI-TOF spectra of (**A**) PEG_{11}-Ts and (**B**) PEG_{21}-Ts. The peaks marked by the blue * arise from the matrix of MALDI-TOF.

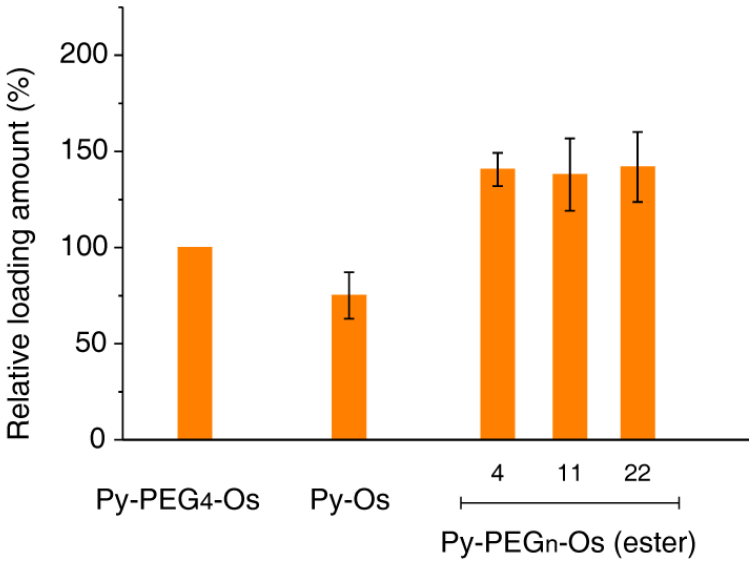

Figure S17. The relative loading amount of Py-PEG$_4$-Os, Py-Os, and Py-PEG$_n$-Os (ester). Molecular probes were loaded on polymersomes in water. A higher loading amount will contribute to a higher packing density of molecular probes on the PEG corona of polymersomes.

S3. Relationship between the conformation of the molecular probe and loading amount

To verify the loading process, we investigated the loading amount of different molecular probes on polymersomes. For Py-Os without PEG spacer, the loading amount was 89±8% of Py-PEG_4-Os (Fig. S17). Electrostatic repulsion between Os was validated to control the packing density of the molecular probe on PEG corona (Fig. S11 and Fig. S14). PEG spacer should provide a larger spacer for the packing of Os, resulting in a higher loading amount of Py-PEG_4-Os than Py-Os. This demonstrated that, besides anchor, PEG spacer could also influence the loading amount of molecular probes due to the electrostatic repulsion between Os.

For Py-PEG_4-Os (ester), the loading amount was 141±9% of Py-PEG_4-Os (Fig. S17), confirming that the linkage between Py and -PEG_4-Os would also influence the loading amount of the molecular probe. The ester group in Py-PEG_4-Os (ester) is more hydrophobic than the ether group in Py-PEG_4-Os, which should increase the binding affinity of Py to PEG corona[8]. The strong interaction between Py and PEG corona overcame the electrostatic repulsion between Os and contribute to the higher loading amount of Py-PEG_4-Os (ester). The loading amount of Py-PEG_4-Os (ester) was close to the loading amount of Py-PEG_4-Os achieved in NaCl solution (141±9% vs 171±24%, Fig. S11). This demonstrated that Py-PEG_4-Os (ester) almost reach the packing density restricted by the steric repulsion between -PEG_4-Os. Moreover, the loading amount of Py-PEG_n-Os (ester) was not influenced by the length of the PEG spacer. Although a longer PEG spacer should contribute to a higher packing density of Py-PEG_n-Os (ester) on PEG corona, the higher steric repulsion of longer PEG spacer should restrict the further increase. The above discussion demonstrated that electrostatic repulsion between Os and van der Waals interaction between Py and PEG corona co-determined the packing density of molecular probe on PEG corona.

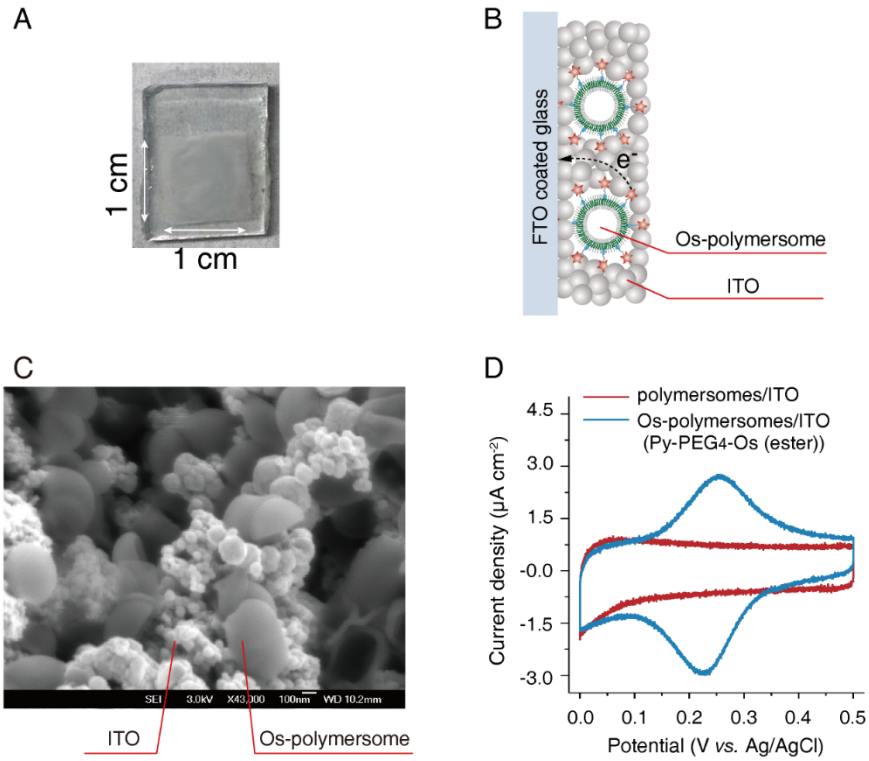

Figure S18. Characterization of working electrode prepared by drop-casting the mixture of ITO nanoparticles and polymersomes modified by Py-PEG$_4$-Os (ester) (Os-polymersomes) onto FTO coated glass. (**A**) The optical image, (**B**) schematic illustration, and (**C**) SEM image of the electrode. (**D**) Cyclic voltammograms of Os-polymersomes/ITO and polymersomes/ITO modified electrode. Redox peaks of Os and the charging current of ITO were detected.

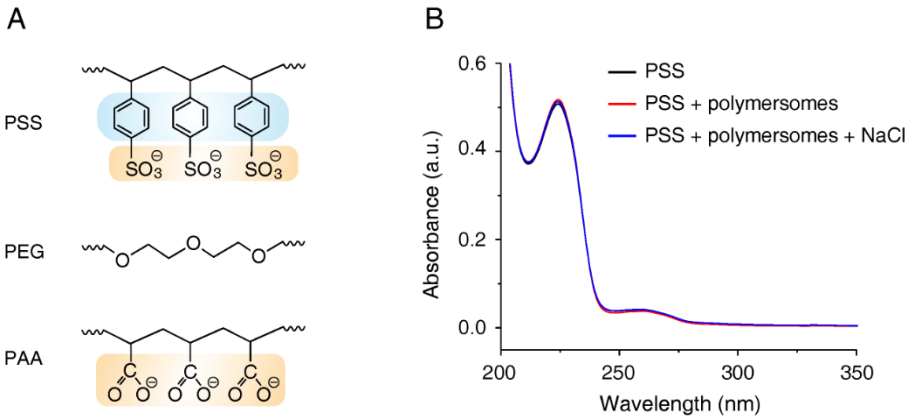

Figure S19. (**A**) Chemical structure of PSS, PEG, and PAA. (**B**) The absorbance of supernatant after adding water, polymersomes, or polymersomes with NaCl into PSS solution. The concentration of polymersomes, PSS (if included), and NaCl (if included) in the solution are 2 mg mL^{-1}, 60 uM, and 10 mM.

Table S1. Thermodynamic parameters for the binding of molecular probes and polymersomes by ITC

Parameter	Ip	Ph	Na	Py
K_d (μM) [a]	0.92	4.4	11	26.7
n [b]	5230	8410	20300	49700
ΔH (kJ/mol) [c]	-3.59	-9.28	-17.2	-17.9
ΔG (kJ/mol) [d]	-34.5	-30.6	-28.3	-26.1
TΔS (kJ/mol) [e]	30.9	21.3	11.2	8.28

[a] K_d, Dissociation constant

[b] n, Binding stoichiometry

[c] ΔH, Enthalpy change

[d] ΔG, Gibbs free energy change

[e] ΔS, Entropy change

References

1. Tu, Y. et al. Self-propelled supramolecular nanomotors with temperature-responsive speed regulation. *Nat. Chem.* **9**, 480-486 (2017).
2. Habermüller, K., Ramanavicius, A., Laurinavicius, V. & Schuhmann, W. An oxygen-insensitive reagentless glucose biosensor based on osmium-complex modified polypyrrole. *Electroanalysis*, **12**, 1383-1389 (2000).
3. Espinoza, E. M. et al. How do amides affect the electronic properties of pyrene? *ACS Omega* **3**, 12857-12867 (2018).
4. Sokol, K. P. et al. Bias-free photoelectrochemical water splitting with photosystem II on a dye-sensitized photoanode wired to hydrogenase. *Nat. Energy* **3**, 944-951 (2018).
5. Ji, X., Wang, W. & Mattoussi, H. Effects of separation distance on the charge transfer interactions in quantum dot-dopamine assemblies. *Phys. Chem. Chem. Phys.* **17**, 10108-10117 (2015).
6. Anet, F. A. L. & Ahmad. M. Restricted rotation in aromatic aldehydes. *J. Am. Chem. Soc.* 86, 119-120 (1964).
7. Keller, S., Teora, S. P., Hu, G. X., Nijemeisland, M. & Wilson, D. A. High-throughput design of biocompatible enzyme-based hydrogel microparticles with autonomous movement. *Angew. Chem. Int. Ed.* **57**, 9814-9817 (2018).
8. Shikata, T. & Okuzono, M. Are all polar molecules hydrophilic? hydration numbers of ketones and esters in aqueous solution. *J. Phys. Chem. B* **117**, 7718-7723 (2013).